SSRG International Journal of Mechanical Engineering
ISSN: 2348-8360/ https://doi.org/10.14445/23488360/IJME-V13I4P105

Volume 13 Issue 4, 62-77, April 2026

Original Article

Bead Morphology Optimization for FLUX Cored Wires in the Wire ARC AM of 1.14 CR-1.0 MO Steel

Vaishali Prajapati[1], Vyomesh Buch[2], Jay Vora[3]

[1,2]*Department of Mechanical Engineering, Parul University, Limda (Waghodia), Vadodara, Gujarat, India.*
[3]*Mechanical, School of Technology, Pandit Deendayal Petroleum University, Gandhinagar, Gujarat, India.*

[1]*Corresponding Author : vaishali.prajapati1@gmail.com*

Received: 10 January 2026 Revised: 20 February 2026 Accepted: 20 March 2026 Published: 29 April 2026

Abstract *- Wire Arc Additive Manufacturing (WAAM), which uses gas metal arc welding, is a promising approach to preparing bulky metal components. WAAM allows consecutive bead deposition for complex forms. The input parameters of the machining process determine deposition quality. The main outputs are Bead Height (BH), Penetration Depth, and Bead Width (BW). This study optimizes Wire Arc Additive Manufacturing (WAAM) parameters for improvement in bead height, Depth of penetration, and bead width. Regression models were tested for adequacy and robustness using variance statistics. Strong model fit was indicated by R^2 and modified R^2 values approaching unity and optimizing used the parameter-free metaheuristic Passing Vehicle Search (PVS) algorithm. Minimum BW was 3.58 mm, maximum BH 6.37 mm, and maximum DOP 1.24 mm were found in multi-objective optimization. The algorithm's efficacy was shown by validation testing, showing disparities between optimized and non-optimized parameters under 5%. Multilayer metal structures were flawlessly produced using these optimal settings. The study provides reliable WAAM parameter sets for high-temperature industrial applications and serves as a baseline for future research.*

Keywords *- GMAW, Flux-Cored Wire, Optimization, PVS Algorithm, Wire Arc AM.*

1. Introduction

AM is a layer-by-layer manufacturing process for complicated, dense metal things with substantial advantages over existing approaches. The system's functionalities are categorized into powder-based and wire-based methodologies, aimed at automating machine mobility, eliminating waste, decreasing energy usage, and enhancing material efficiency [1-3]. Powder-feed and wire-feed techniques are two popular added material supply systems. The small size and great geometrical accuracy provided by powder feed, whereas wire-feed is cleaner, more environmentally friendly, and more material efficient. Because of the availability of metal wires, it has also reduced expenses and is more cost-competitive [4-6]. Because wire-arc additive manufacturing requires post-processing to keep the original parts, it is critical to limit post-processing. The process productivity is assessed through the buy-to-fly ratio [7]. Zhong et al. [8] revealed that 3D metal printing processes, with a focus on GMAW-based WAAM, are more convenient and easier to manufacture.

Szost et al. [9] discovered that good design variable selection and parametric optimization reduce residual stresses and distortion. WAAM, according to Tabernero et al. [10], revealed that it is appropriate for producing larger components at lower costs using materials such as steel alloy, Ti alloys, Ni alloys, aluminum, and bronze. For accuracy, WAAM requires an arc generator, a wire feed system, and a substrate. Lockett et al. [11] gave design criteria for producing aerostructure parts, whereas Bushachi et al. [12] investigated the procedure path for military platforms. Yuan et al. [13] investigated a system for architectural beading positioning, optimization process parameters for multidirectional. Lockett et al. [11] provided design principles and assessment procedures for generating aerostructure parts and determining construction characteristics. To calculate the best path shape and welding conditions, they created a parabola model. According to the study, selecting process parameters and their needed levels is critical for depositing numerous layers of WAAM, with optimization attempts for different steels. For high-pressure and high-temperature fabrication applications, alloy steel (1.14-Cr-0.5 Mo) is suitable. They demonstrate excellent weldability within the temperature range between 370°C to 550°C, but extended exposure to these temperatures can cause embrittlement. Gas flux arc welding usually employs a solid wire, However, employing tubular core wire can improve current density and deposition rate.

The protective layer of Core flux can supplement flux-cored wires. It has better productivity and faster welding of thicker materials than solid wires. Flux-core (WAAM) is a suitable welding wire for environmentally sensitive areas, high-strength mechanical joints, versatility, high-temperature tolerance, and corrosion resistance. It creates less porosity, more flexibility with material composition, and molten pool reinforcement [14]. Metal core wire exhibits limitations in its application to thin materials,

presents challenges in achieving full penetration welds, and demonstrates reduced flexibility. Additionally, the efficiency of flux-cored wires is enhanced by the increase in deposition and current density [15, 16]. Several meta-heuristics strategies have been used to improve welding parameters in a variety of applications. Zequi Hu et al. [17] examined genetic algorithms from two models and Artificial Neural Networks to see which one outperformed the backward Artificial Neural Network (BANN). The FANN-GA model produced less splatter and a better bead appearance than the BANN model. L. Wang et al. [18] revealed that Wire arc AM tests on stainless steel 316L material and discovered that the speed arc and speed pulse production techniques were stable and efficient. Speed Arc WAAM's finer solidification structure and lower heat input resulted in greater hardness and tensile strength than Speed Pulse WAAM. M. Wash et al. [19] employed Wire Arc AM to produce aluminum products utilizing gas metal arc with structural incorruptibility of aluminum products utilizing pulsed gas metal arc welding while keeping heat input low. Lei Yuan and Dong Hong Ding [13] created a multidirectional WAAM technique that resulted in a 52% reduction in production time, a 57% material costing decreased, and a 57% miniaturized in material utilization. The parabola bead model was utilized to create the necessary bead shape, and CMT was chosen for welding deposition due to its low heat input and short arc transfer characteristics.

Subhash et al. [20] studied the potential for temper embrittlement in a 1.25Cr-1.0 Mo welded joint treated with step cooling treatment, necessitating additional examination, and provided a foundation for the utilization of metal-core wire. kumar et al. (2021). Selected variables for individual metal bead deposition utilizing the gas-based metals arc welding method are being investigated and observing ferrite with pearlite structures around the welded region, as well as fractures and porosity caused by increased deposition height. Figure 1 shows the AM material types.

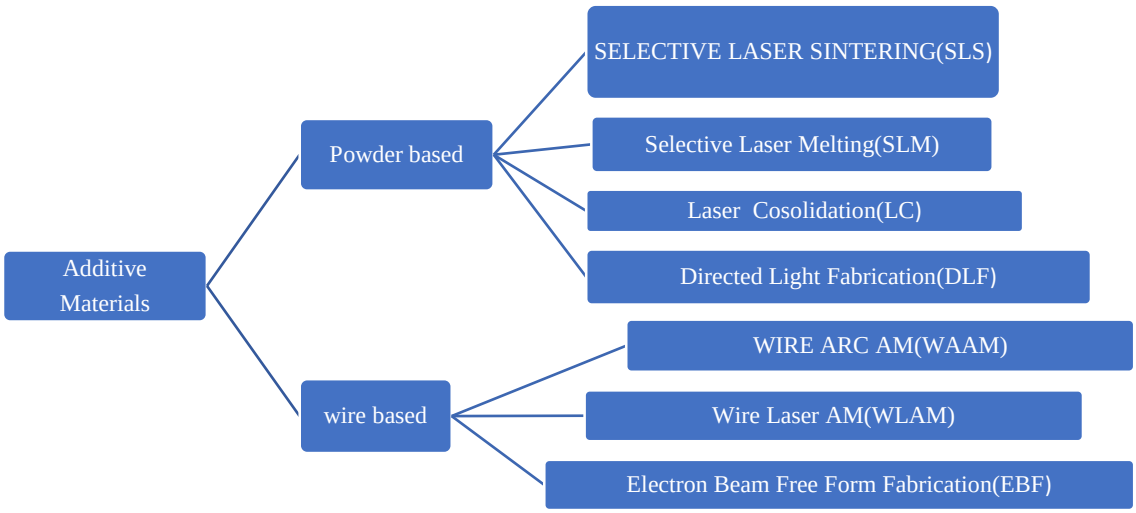

Fig. 1 AM material types [14]

The metal additive materials are classified based on powder and wire-based materials. Wire AM generated from the feedstock is quickly added to the pool of molten metal that the original has created, enabling successive layers of wire melting in either the absence of air or a shielding gas chamber. GMAW, based on WAAM, utilizes a simple tool path with a planning algorithm, lower cost, and a user-friendly interface for greater convenience in utilizing heat sources. However, the WAAM process has a strong correlation between deposition speed and the overall quality of manufactured parts [21, 22].

The wire feeding technique is a safer method with reduced harmful powder absorption. It provides low wire material waste. The wire-feeding technique is a more ecologically friendly and efficient technology. that shields employees from possibly risky powder situations. It uses materials more efficiently than the powder-feed method, as much as one hundred percent of the wire's element is incorporated into the component. Moreover, metal wires are affordable and easier to acquire than metal powders with properties suitable for additive manufacturing, making the wire- feeding approach more economical. However, WAAM machine input parameters are challenging for the microstructure effect, which can cause the heat-affected zone. Therefore, parameter optimization is required to improve the effects of metallurgy [23-25].

The previous research and review articles on WAAM have focused on process control, optimization of deposition parameters, and sensing. Also, research endeavors have neglected to investigate the distinctions between metal core wire and flux core wire. It is imperative to address this gap in knowledge to achieve a comprehensive understanding of welding processes. We propose to undertake this important research to bridge this gap in the literature.

Differentiated evolution, particle swarm optimization, and cuckoo search algorithms are used to solve complex problems through optimization techniques. Still, these algorithms exhibit deficiencies in the genetic algorithm,

especially a lack of localization capabilities and slow convergence speed [26, 27]. PVS is an algorithm-parameter-free meta-heuristic optimization technique.

This article presents recent research on new materials and machining armatures using a new optimization algorithm strategy. The current environment necessitates the use of ready-to-use products to minimize time consumption; hence, WAAM is a form of additive manufacturing procedure that fulfills contemporary requirements. In all works we found Metal core wire with WAAM, but flux cored wire is rarely utilized, so this one is actually a novelty of work. In most studies, we observed the use of metal core wire using Wire Arc Additive Manufacturing (WAAM), but flux-cored wire is seldom used; hence, this represents a new aspect of the research.

The low steel alloy on a base plate to optimize the post-processing and void. To achieve this, overlapping parameters, multiple-layer thickness deposition, bead height, Depth of penetration, and bead width were all considered simultaneously. The input process parameters chosen were voltage, travel speed, and gas mixture, whereas the output process parameters were bead width, Depth of penetration, and bead height. The regression equations were subjected to ANOVA to test for robustness and appropriateness. The novel metaheuristic algorithm technique was used for multi-optimization with multiple objectives, generating response Pareto fronts. The authors have discovered the optimal conditions for depositing layer flux, which they believe has significant industrial applications.

2. Research Strategy and Flow Chart

The purpose of our current research is the optimization of parameters associated with the process. The voltage, travel speed, and gas mixture as input parameters, given their compatibility with the machine's capabilities and effects of these process parameters at three distinct levels of machining variables, utilizing Response Surface Methodology (RSM). A total of 15 experiments were performed for the analysis. The experimental equipment used to demonstrate the Wire Arc Manufacturing (WAM) by the additive manufacturing technique is presented in Figure 2. Corresponding to this setup are various experimental parameters, each with its own respective level. The parameters were chosen considering their significant impact on the weld bead and ultimate structural shape in industrial applications. These parameters and their corresponding levels are outlined in detail in Tables 1 and 2.

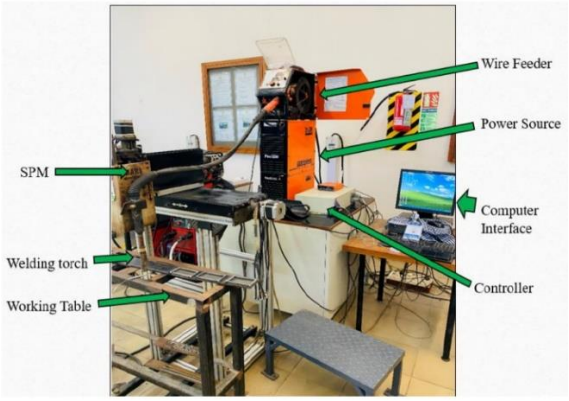

Fig. 2 WAAM experimental setup [15]

Table 1. Experimental parameters and levels

Parameters	Values
Voltage	20;23;26 V
Travel speed (mm/min)	20;25;30 mm/min
Gas mixture	1,5,9
Flow rate (gas)	15 L/min
Length of Arc	90 mm

Table 2. Design of experiment

Number	Voltage(V)	Travel speed(m/min)	Gas mixture(L/min)
1	23	20	9
2	23	25	5
3	26	25	1
4	20	30	5
5	26	20	5
6	20	25	9
7	26	30	5
8	23	30	1
9	23	20	1
10	23	30	9
11	20	25	1
12	23	25	5
13	26	25	9
14	20	20	5
15	23	25	5

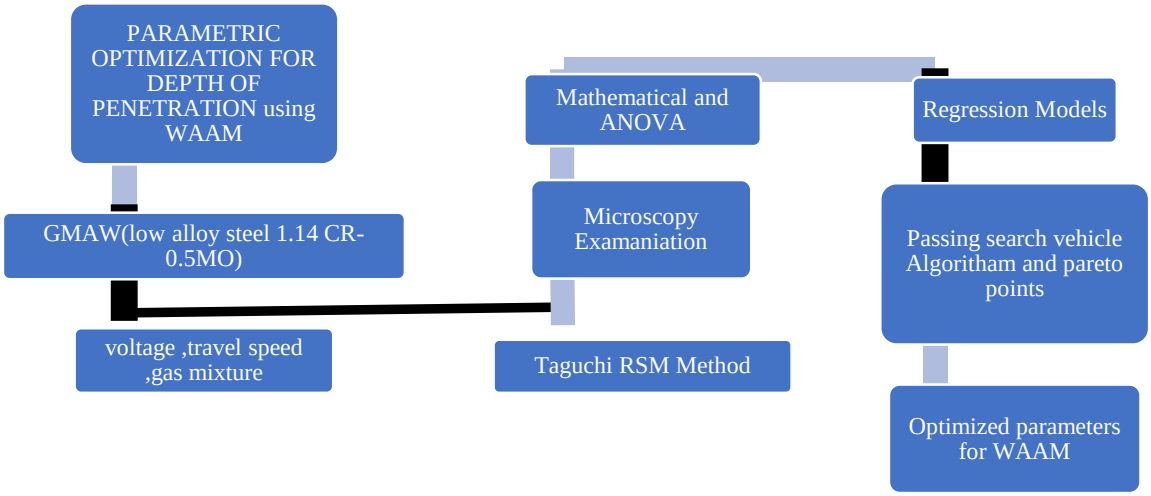

Fig. 3 Proposed research flow chart

The proposed flow chart for research methodology and optimization techniques, as well as the resulting optimized WAAM parameters, are shown in Figure 3.

2.1. Materials and Methods

This study examines the use of flux-core wire in wire arc additive manufacturing for a 1.14 Cr-0.5Mo steel alloy. Specifically, the study employs E81T1-B6 wire, provided by TRI-MARK with a 1.14mm diameter, which is typically used for welding chromoly steels in multiple or multi-pass welding. The cleaning regime of making the surface free of rust by either grinding with a wire brush and emery paper was conducted, followed by cleaning with acetone.

The experimental setup comprises a PRO MIG-530 Gas Flux Arc Welding (GMAW) system from Miller, using a shielding gas with varying mixture ratios. The study conducts bead-on-plate experiments on a base plate with voltage, traveling speed, and gas flow rate as input parameters. The validity and suitability of regression formulas are assessed through analysis of variance (ANOVA). The research utilizes the Passing-vehicle-search optimization method for optimizing both single and multiple responses for Bead Width (BW) and Bead Height (BH). Furthermore, the study develops Pareto fronts to provide a unique, non-dominated solution. The experiment validated and demonstrated the appropriateness of the algorithm. The parameters are further refined to determine the most effective parameters for single-layer flux deposition. Table 3 presents the material composition of the wire, which is used as a base plate for this study, which was carried out using a PRO MIG-530 GMAW setup from Miller.

Table 3. 1.14 mm E81T1-B6C/M 4-6 % cr 0.45-0.65% molybdenum chemical composition

Grade	C	Mn	Si	P	S	Cr	Ni	Mo
	0.06	0.29	0.36	0.007	0.011	4.45	0.05	0.48

During the welding process of low alloy steel with a 1.14Cr-0.5Mo substrate, flux-cored wires were utilized. The welding process, known as WAAM, employed Met alloy wire with flux-cored having a 1.14 mm diameter, manufactured by Hobart Brothers (TRI-MARK).

Typically used for welding chromoly steels in single or multi-pass applications, the welding technique involved the use of shielding gas at rates of 1, 5, and 9 L/min.

2.2. Optimization Using the PVS Algorithm

An optimization algorithm named passing vehicle search (PVS) was developed for the parking vehicle searching and navigation process for highway lanes. It belongs to the class of human activity-based meta-heuristics, which aim to discover optimized solutions for a function. Engineering problem challenges demonstrate PVS efficiency. It has the ability to find a solution for different computational runs and times. [28].

Throughout the execution of the PVS algorithm, every outcome is considered a positive integer. Constraints specified for the optimization approach pertain to Voltage (V), Traveling Speed (TS), and Gas Mixture Ratio (GMR) of the system. Where $20 \leq TS \leq 30$, $20 \leq V \leq 26$, and $1 \leq GMR \leq 9$.

In order to optimize individual responses, a higher value of d bead Height and Depth of penetration was considered, while lower values were considered for Bead Width. Importantly, all output variables should be considered positive integers for implementation. The table labeled as Table 4 displays the results of an optimization objective.

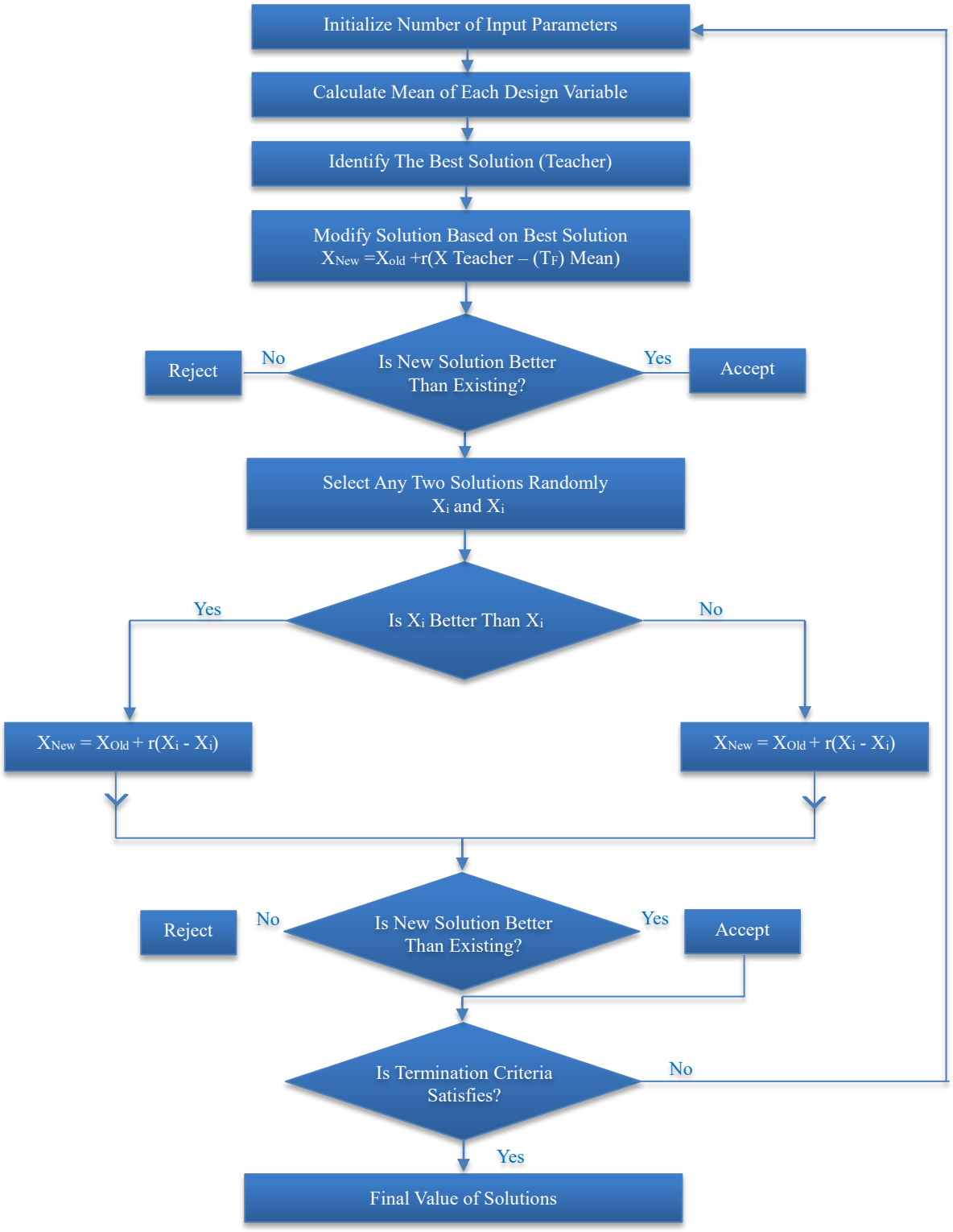

Fig. 4 Optimization PVS algorithm

Table 4. Optimization objective with the PVS method

	Design variables			Objective function		
Function objective	**Travel speed**	**Voltage**	**GMR**	**Bead Height**	**Minimum Width**	**Maximum DOP**
Maximum bead Height	30	26	1	6.37618	4.67512	4.67512
Minimum Width	30	20	9	4.2896	3.5864	1.189064
Maximum DOP	30	20	1	4.5001	3.9754	1.249549

During the PVS algorithm, four different cases were thought of. Each case had different objectives and constraints. Case I aimed to maximize the bead height, Case II aimed to minimize the bead height with high accuracy, Case II aimed to get maximum DOP, and Case IV was the optimal case that combined all three objectives. In summary, the implementation of the PVS algorithm followed strict rules device bounds to optimize individual responses. The algorithm considered all output variables as positive integers, and four different cases were thought of to achieve different objectives. It is important to consider that the optimization process can be tailored to specific objectives and constraints to achieve optimal results.

Case I: Obj. = max. (Bead Height)					
TS=30	V=26	GMR=1	BH=6.37618	BW=4.67512	DOP=1.142671
Case II: Obj. = min (Bead Width)					
TS=30	V=20	GMR=6	BH=4.2896	BW=3.5864	DOP=1.189064
Case III: Obj. = max (DOP)					
TS=30	V=20	GMR=1	BH=4.5001	BW=3.9754	DOP=1.249549
Case IV: Obj. = w1 (BH) + w2 (BW) + w3 (DOP)					
TS=30	V=23	GMR=3	BH=5.26307	BW=4.17218	DOP=1.172924

3. Results and Discussion

This section presents the findings from experiments with optimization techniques and optical microscopy, which can display the optimized input parameters for achieving good bead morphology. Table 5 and Figure 5 present the experimental matrix, input process parameters, and measured outcome parameters for bead height, penetration depth, and height using the Box-Behnken design. The results show that the validation trials experiment discussed that due to different uncontrollable parameters, the exact match between predicted and experimentally measured values always occurs. However, the difference is very small and can be ignored. Multivariable correlations were applied to analyze the responses within the range of the design variables. The findings of this study offer a correlation between the variables of the design and the responses, which will do future research and development efforts.

Table 5. BW and BH response surface method BBD design

Std Order	Run Order	Voltage(V)	Travel speed(m/min)	Gas mixture	Depth of Penetration (DOP) (mm)	Bead Height (BH) (mm)	Bead Width BW (mm)
11	1	23	20	9	0.734	3.970	7.158
14	2	23	25	5	0.668	5.200	7.685
6	3	26	25	1	0.820	5.392	6.125
3	4	20	30	5	0.506	6.152	9.546
2	5	26	20	5	0.880	3.976	5.765
7	6	20	25	9	0.654	5.398	10.344
4	7	26	30	5	0.784	6.139	6.371
10	8	23	30	1	0.558	6.770	8.371
9	9	23	20	1	0.712	3.287	6.595
12	10	23	30	9	0.758	6.184	8.900
5	11	20	25	1	0.552	4.237	8.856
13	12	23	25	5	0.650	4.864	7.944
8	13	26	25	9	0.878	5.485	6.678
1	14	20	20	5	0.589	3.900	8.464
15	15	23	25	5	0.655	5.136	7.711

(a) Workpiece RO 6

(b) Workpiece RO 8

(c) Workpiece RO 13

(d) Workpiece RO 11

(e) Workpiece RO 9

(f) Workpiece RO 5

Fig. 5(a-f) WAAM workpiece RO 6,8,13,11,9 and 5.

The presented data depict that the Run Order (RO) 6 yields a superior Bandwidth (BW) at 20 V, speed of 25 m/min, and a gas mixture of 9 L/min, while the RO 8 exhibits a higher Bead Height (BH) at 23 V, travel speed of 30 m/min, and a gas mixture of 1 L/min. Moreover, RO 13 demonstrates a more significant Drop of Penetration (DOP) performance at 26 V, travel speed of 25 m/min, and gas mixture of 9 L/min. These findings are valuable for determining the optimal parameters for maximizing the desired outcome in the relevant manufacturing process. The RO 11 model exhibits a lower DOP when operated at 20V voltage, 25 m/min travel speed, and a gas mixture of 1 L/min. In contrast, the RO 9 model displays a lower BH when operated with 23V voltage, 20 m/min travel speed, and a gas mixture of 1 L/min. The RO 5 model demonstrates a lower BW when operated at 26V voltage, 20 m/min travel speed, and a gas mixture of 5 L/min. However, these parameters influence the weld bead. Some parameters gave smooth morphology, and some gave excellent morphology. The data from those trials were fed into the PVS algorithm, and then an optimum parameter was finalized. The WAAM layer-by-layer deposition was not done on any of these trials, but on the optimum parameter setting obtained from the output of the algorithm.

3.1. Mathematical Modeling and ANOVA

The mathematical regression analysis uses Response Surface Methodology, which is widely used for analyzing response variables. For the regression equation for bead width and height, we utilized Minitab v17. The resulting equations (1), (2), and (3) for BW and BH incorporate the following variables: Voltage (V), Traveling Speed (TS), and Gas Mixture Ratio (GMR). These equations comprehensively understand the correlation between input and outcome variables.

$$BH = 7.8 + 0.074 * V + 0.466 * TS + 0.928 * GMR + 0.0028 * V * V - 0.00201 * TS * TS + 0.0023 * GMR * GMR - 0.0015 * V * TS - 0.0223 * V * GMR - 0.01586 * TS * GMR \quad (1)$$

$$BW = 3.2 - 0.219 * V + 0.803 * TS + 0.419 * GMR + 0.0001 * V * V - 0.00976 * TS * TS + 0.0138 * GMR * GMR - 0.0079 * V * TS - 0.0195 * V * GMR - 0.00042 * TS * GMR \quad (2)$$

$$DOP = 1.820 - 0.1185 * \mathrm{V} - 0.0104 * \mathrm{TS} - 0.0442 * \mathrm{GMR} + 0.00375 * \mathrm{V} * \mathrm{V} - 0.000068 * \mathrm{TS} * \mathrm{TS} + 0.002159 * \mathrm{GMR} * \mathrm{GMR} - 0.000217 * \mathrm{V} * \mathrm{TS} - 0.000917 * \mathrm{V} * \mathrm{GMR} + 0.002225 * \mathrm{TS} * \mathrm{GMR} \quad (3)$$

Table 6. (a, b, and c) RSM (ANOVA) for BH, BH, and DOP

Source	DF	SS	MS	F	P	Significance
(a) RSM (ANOVA) for DOP						
Model	9	0.187506	0.020834	61.48	0.000	Significant
Linear	3	0.170891	0.056964	168.09	0.000	Significant
Voltage	1	0.140715	0.140715	415.23	0.000	Significant
Square	3	0.008168	0.002723	8.03	0.023	Non- Significant
Interaction	3	0.008447	0.002816	8.31	0.022	Non- Significant
Error	5	0.001694	0.000339			
Lack-of-Fit	3	0.001522	0.000507	5.88	0.149	Non- Significant
Pure Error	2	0.000173	0.000086			
Total	14	0.189200				
Source	**DF**	**SS**	**MS**	**F**	**P**	**Significance**

(b) RSM (ANOVA) for BH						
Model	9	13.9301	1.5478	12.69	0.006	Significant
Linear	3	13.2226	4.4075	36.13	0.001	Significant
Square	3	0.0178	0.0059	0.05	0.984	Non- Significant
Interaction	3	0.6897	0.2299	1.88	0.250	Non- Significant
Error	5	0.6100	0.1220			
Lack-of-Fit	3	0.5465	0.1822	5.74	0.152	Non- Significant
Pure Error	2	0.0635	0.0317			
Total	14	14.5401				
Source	**DF**	**SS**	**MS**	**F**	**P**	**Significance**
(c) RSM (ANOVA) for BW						
Model	9	24.1445	2.6827	22.13	0.002	Significant
Linear	3	23.4369	7.8123	64.45	0.000	Significant
Square	3	0.4321	0.1440	1.19	0.403	Non- Significant
Interaction	3	0.2755	0.0918	0.76	0.564	Non- Significant
Error	5	0.6061	0.1212			
Lack-of-Fit	3	0.5654	0.1885	9.27	0.099	Non-Significant
Pure Error	2	0.0407	0.0203			
Total	14	24.7506				

Table 6 shows (a, b, and c) RSM (ANOVA) for BH, BH, and DOP. The regression equations resulting from the study were subjected to rigorous testing for robustness and appropriateness through analysis of covariance. Table 4 presents an analysis of the results of the covariance outcomes. In addition, analysis of covariance was found to be non-significant, and significant models with respect to bead width and bead height. The approach was evaluated on 95% level of significance to determine its validity. The p-value is significant, and the suggested model has less than 0.05 with observed response values. The model terms demonstrate an elevated F-value within 95% confidence range and a reduced probability p-value (below 5%). The regression model of BW, comprising linear, square, and interaction factors, reports significant results with a p-value below 5 percentage. Both the regression and linear models had a considerable influence on determining the BH reaction. The model created is highly accurate in predicting responses with minimal error, as evidenced by the small contribution of error components for both responses.

Meanwhile, non-significant Analyses of covariance results do not fit the predicted response value. The established model terms exhibit a high degree of significance, indicating that the resulting regression equations are reliable and can be used to predict future BW, DOP, and BH values. The model's adequacy was evaluated through R2 values, indicating its capacity to predict future observations accurately.

Specifically, the R2 value for DOP was found to be 0.9749, while the R2 values for BH as well as BW were 0.9580 and 0.9314, respectively. Additionally, the BH had an R2 value of 0.9356. The favorable R2 and adj. R2 values for DOP, BW, and BH affirm that the model is suitable for the present data and can be used to predict future observations accurately.

3.2. Main Effects Plot for DOP, BH, and BW

Travel speed, along with heat, is an important process parameter. The voltage controls the heat to regulate the amount of heat, which influences the deposition of the weld. The WAAM machine outcomes are measured based on the DOP, BW, and BH parameters. Figure 6 displays the primary effect plot for DOP, BW, and BH, which explains the observed trend when adjusting the feed speed of wire, speed of travel, and voltage. The graph indicates an increase in BW as the travel speed increases. This is due to the torch's rapid deposition of particles. As the torch's speed increased, fewer molten flux drops were deposited, reducing the weld bead's width [19].

Moreover, the voltage trend indicates an increase in the Weld Bead's BW. The broadening of the arc caused larger droplets of molten flux to be deposited, leading to a rise in the bead. As a result, bead width has a positive impact. On the other hand, increasing the wire feed speed has an adverse effect as the width decreases.

The increase in BW is attributed to the speed of the wire leaving the nozzle and the amount of deposited material. The main effect plot is represented in Figure 4 of penetration depth, bead width, and BH effect of varying voltage, travel speed, and gas mixture. The voltage affects DOP, BH, and BW. The DOP increases with voltage, and the gas mixture increases and decreases with travel speed.

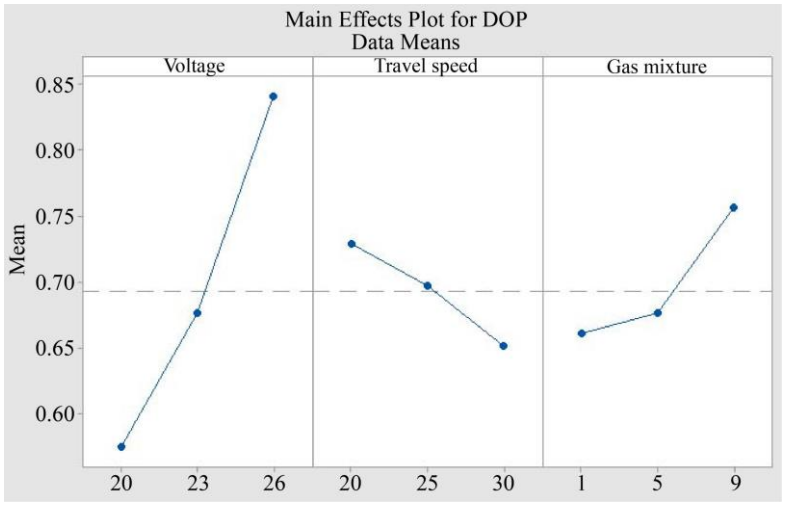

(a)

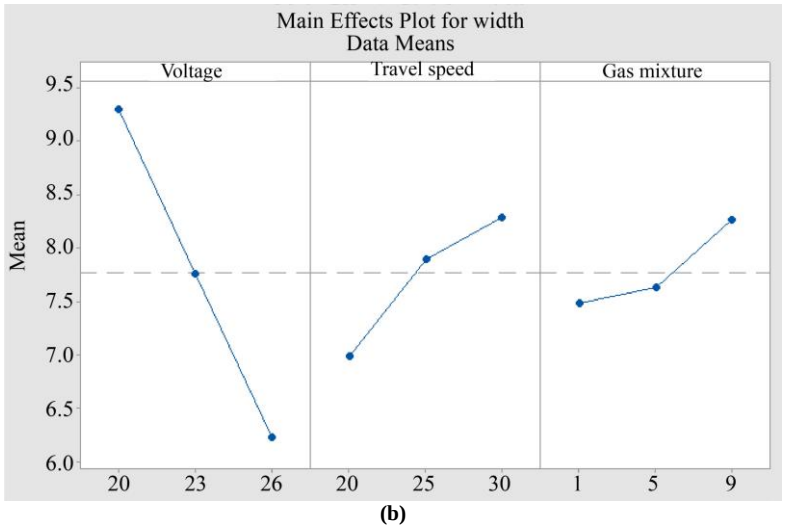

(b)

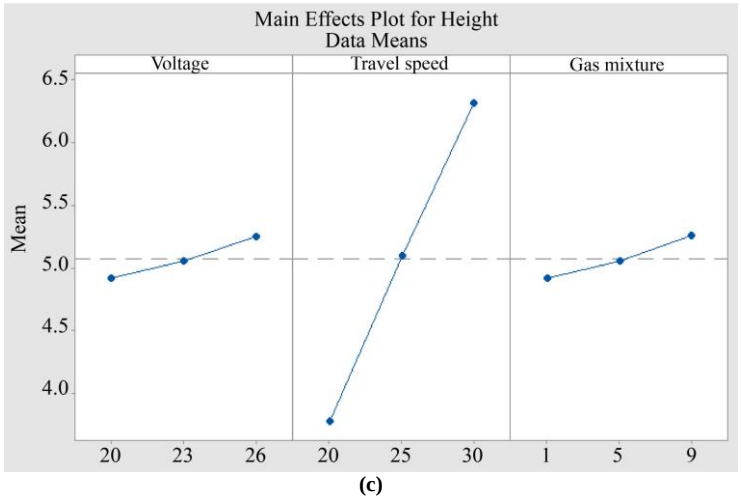

(c)

Fig. 6 Main effect plots for (a) DOP, (b) BW, and (C) BH.

3.3. Residual Plots

The validity of an ANOVA analysis rests on the fulfillment of specific assumptions, as indicated by residual plots. In particular, residual plots for Bead Width, DOP, and Bead height presented in Figure 5, each comprises four plots. Of these, the normalcy plot is particularly informative, as it provides evidence of a linear progression and thus confirms the model's appropriateness. [29]. The second plot, depicting the fits, exhibits a random distribution around the source, while the histogram demonstrates a bell-shaped curve, thereby bolstering the outstanding ANOVA results. The lack of trend in the plot supports the ANOVA statistics. All four graphs validate the ANOVA statistics, resulting in more accurate forecasts of future outcomes.

A similar outcome was observed for BH, as presented in Figure 7. The ANOVA statistics were substantiated by all four plots, thus augmenting the accuracy of predictions for future BW and BH findings. The normal probability curve, known as the inverted S-curve, implies a distribution with both short tails and long tails. The residual observation order trend shows cyclic variation and a shift with both negative and positive residuals. All variance plots show similar patterns, and no concerning trends are present. The residual for DOP and BH is better and fits a normal distribution, while the BW residual is the closest fit to a normal distribution.

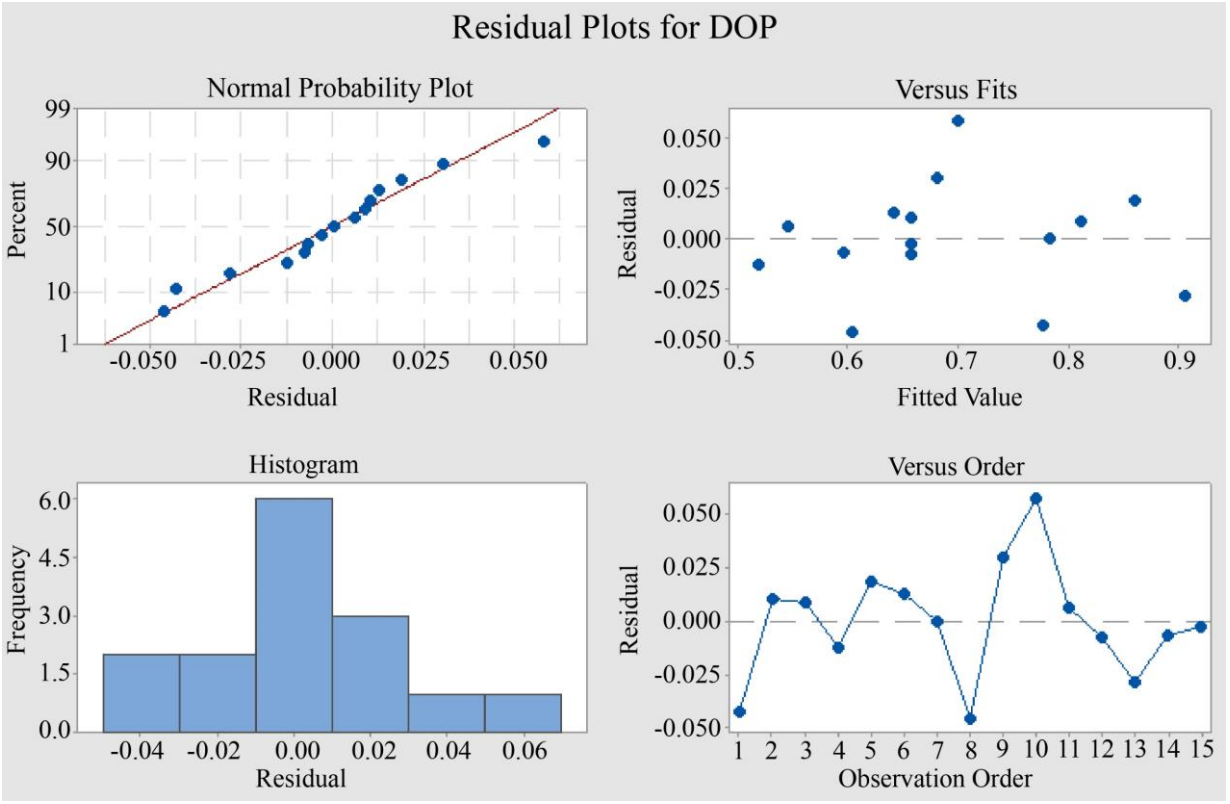

(a)

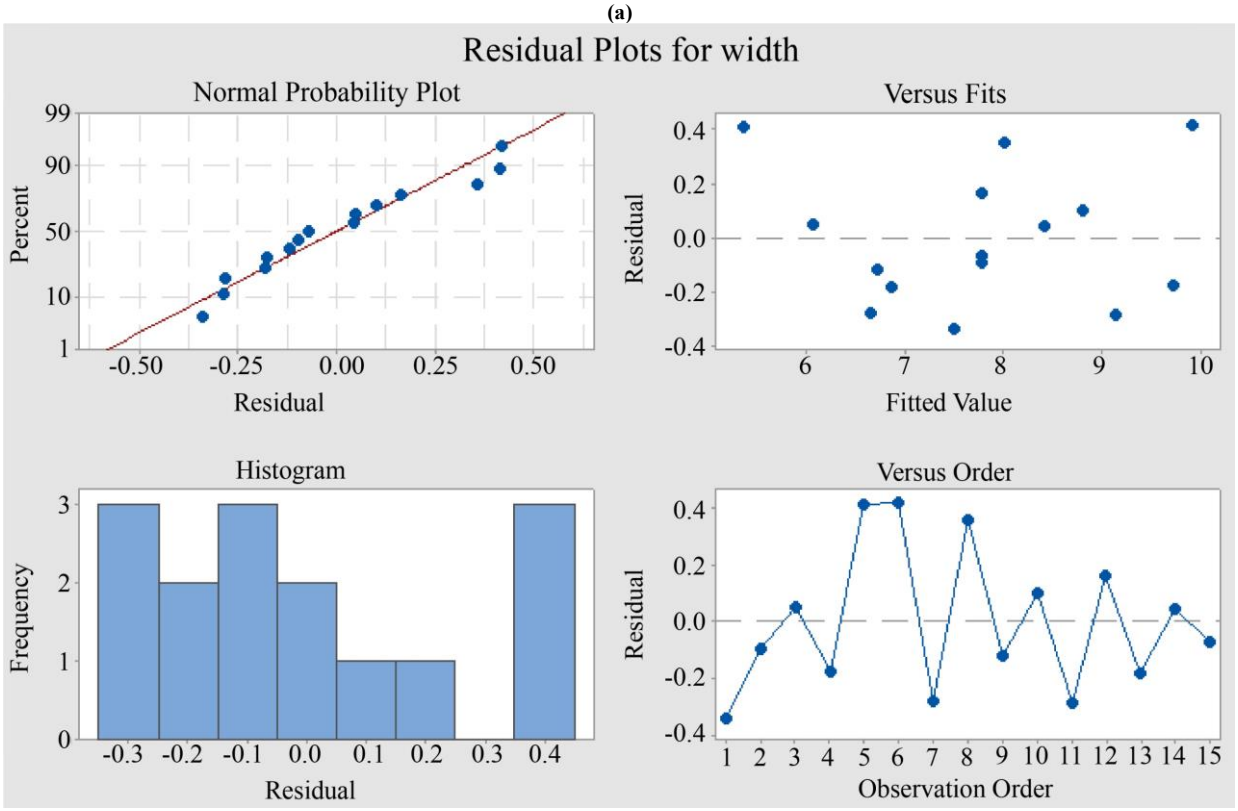

(b)

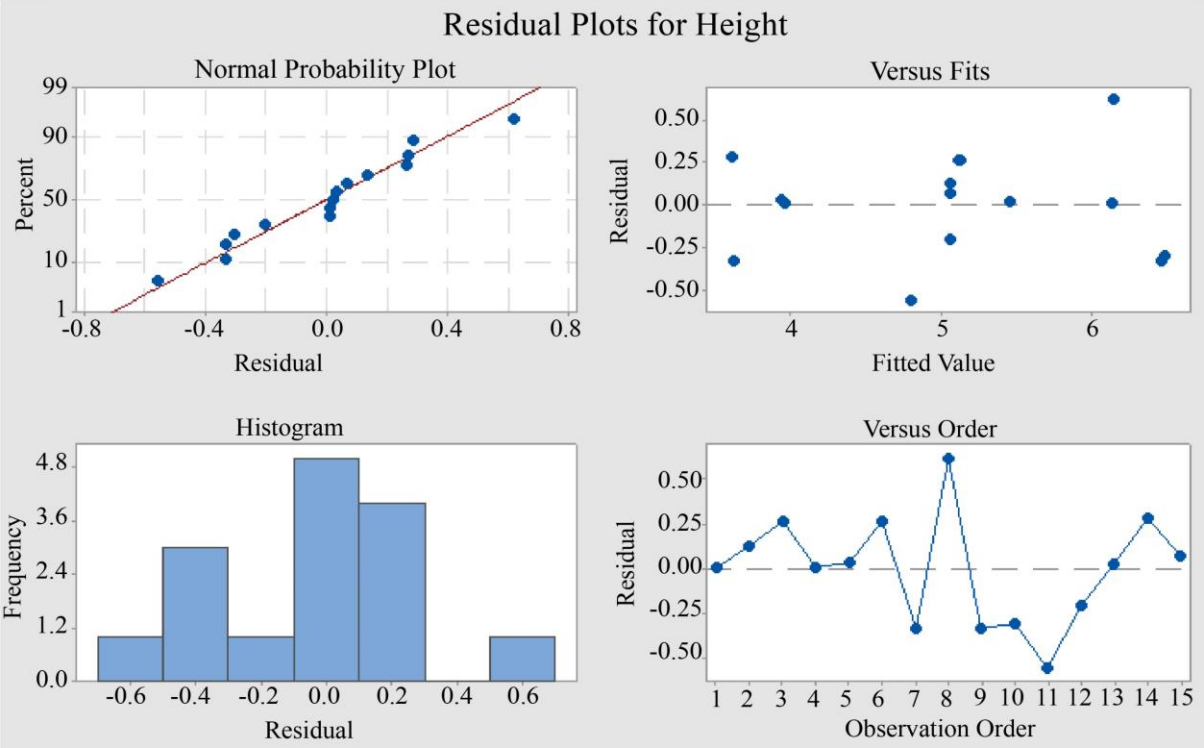

(c)

Fig. 7 Residual plots for (a) DOP, (b) width, and (c) height.

3.4. Optimization using Pareto Points and Optical Microscopy

In multi-objective optimization problems, Pareto sets are used. These are efficient frontiers of solutions in the performance space. Pareto sets present two main challenges: populating the set with solutions and selecting the best solution from the set. These challenges are similar to the ones faced in decision-based design, where potential solutions need to be determined and selected. However, in Pareto analysis, there are additional criteria that must be met for a solution to be included in the set. The design vector X* is calculated as an optimum Pareto vector that satisfies the criteria with x. [30]. Table 4 below shows the optimization of Pareto points. This analysis examines the distribution of benefits in the context of multiple objectives. The Pareto optimization concept of identifying workable mathematical solutions. It can be helpful for subpopulation and conductance-based models for minimizing each objective function without compromising at least one of the other objectives.

The Pareto optimality criterion aims to find solutions that offer the best trade-offs among different objectives while avoiding any degradation of any of them. Table 7 (supplementary material) and Figures 8, 9 and 10 present the results of the optimization process, which highlight the most efficient solutions. The analysis of Pareto points optimization is essential in various fields, including business and engineering, where it is typically used to optimize complex systems.

$$f_i(x) \leq f_{i\,(x^*),j=1\ldots,m} \text{ and } f_i(x) \leq f_{i\,(x^*)\ for\ a\ last\ one\ i\ \ 1\leq i\leq m} \quad (4)$$

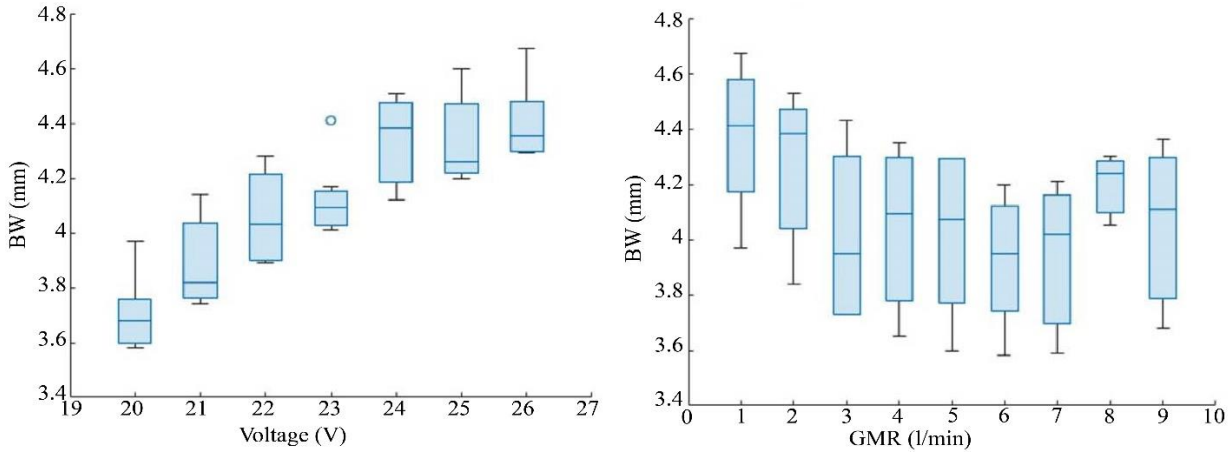

(a) **(b)**

Fig. 8 Plot of (a) BW vs Voltage and (b) BW vs GMR

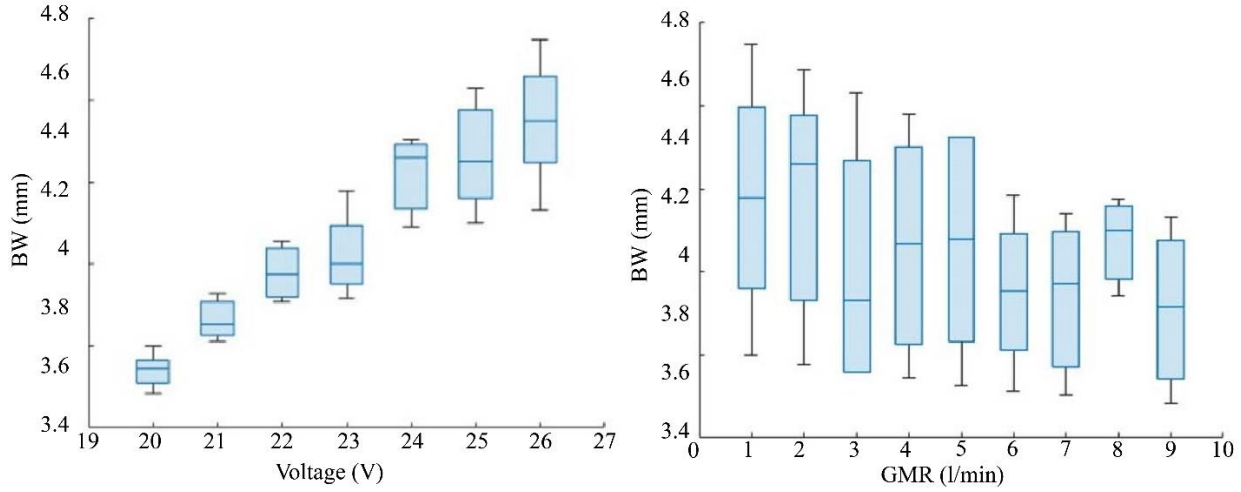

(a) **(b)**

Fig. 9 Plot of (a) BH vs Voltage and (b) BH vs GMR

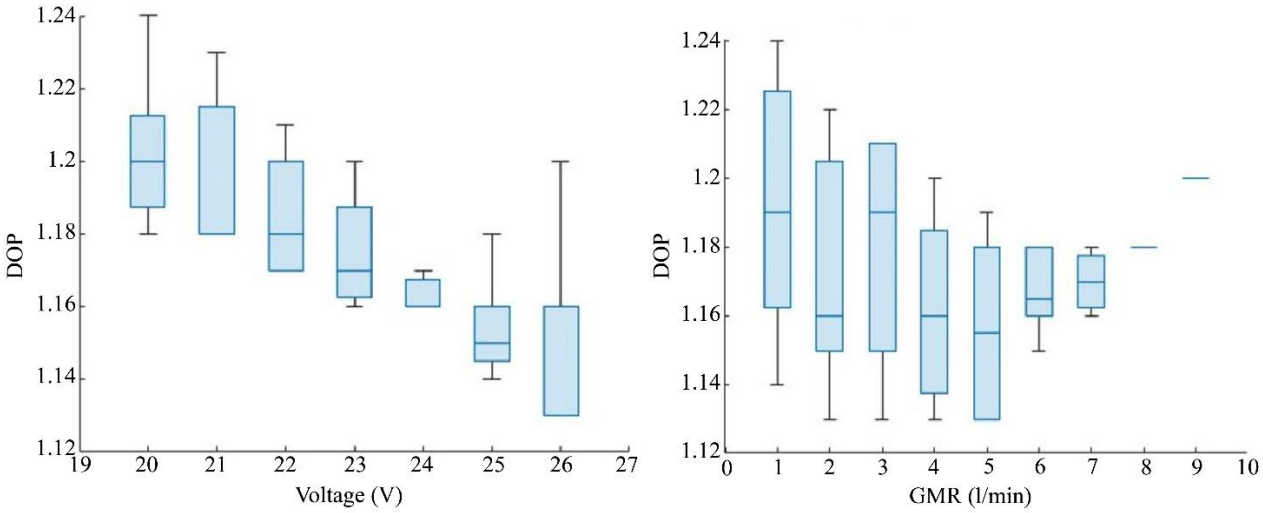

(a) **(b)**

Fig. 10 Plot of (a) DOP vs Voltage and (b) DOP vs GMR

The BH and BW values are elevated at 26 volts and 1 GMR 1, whereas the DOP values become higher at 20 volts and GMR 1. Although a uniform transit speed of 30 m/min is upheld at all locations, identifying the ideal position remains difficult owing to these fluctuations. Manufacturers may choose any place on the front, as it represents an arrangement between two opposing aims.

The impact of the aforementioned variables on the bead height and width was studied, with each bead's BH and BW deposition scrutinized through optical microscopy. The average value of each experiment was recorded for further analysis. The optimal micrographs of the specimens can be viewed in Figure 11 (A-). The sample 1 BH measures 5.18 mm in height and 3.97 mm in width. The voltage is 23 V, and the gas mixture ratio is high. The shape is not circular, leading to the creation of a heat-affected zone. Sample 2 has a width of 8.50mm, a height of 7.43mm, and a depth of 0.66 mm, creating a heat-affected zone. Sample 4 measures 6.81 mm in width, 5.12 mm in height, and has a created surface unmixed zone. Sample 5 has an elliptical shape. \Sample 6 has a base width of 9.34 mm and a height of 5.57 mm, with a DOP of 0.88 mm. Sample 8 has a base width of 9.75 mm and a base height of 5.67 mm—an additional 0.90 mm DOP at 26 V and 30 m/min. Sample 9 has a BW of 6.85 mm and a BH of 5.87 mm, with 0.50 mm melted at 23 V and 30 m/min. Sample 10 has 0.68 mm DOP at 23 V and 20 m/min, and the BW is 4.47 mm and BH 4.67 mm. However, BH and BW still need to be more than required. Sample 11 has a width of 7.63 mm and a height of 5.37 mm with 0.23 mm DOP at 23 V and 30 m/min, causing HAZ. Sample 12 has an unmixed zone forming. Sample 13 has an additional 0.52 mm melted at 23 V and 25 m/min, resulting in excessive spatter in the heat-affected zone. However, the HAZ is reduced. Sample 15 has a 5.25 mm width and a 5.25 mm height, indicating a good circular shape with minimal HAZ.

The PVS algorithm's optimum parameter outcomes are shown in Table 7. It is an optimal condition for depositing the flux layer for industrial applications.

Table 7. BW and BH optimized values

Optimization Type	Process parameters			Responses		
	Voltage (V)	Travel speed (m/min)	Gas mixture (L/min)	BH (mm)	Minimum BW (mm)	Maximum DOP (mm)
Maximization of BH	26	30	1	6.37618	4.67512	4.67512
Minimization of BW	20	30	9	4.2896	3.5864	1.18906
Maximization of DOP	20	30	1	4.5001	3.9754	1.2495

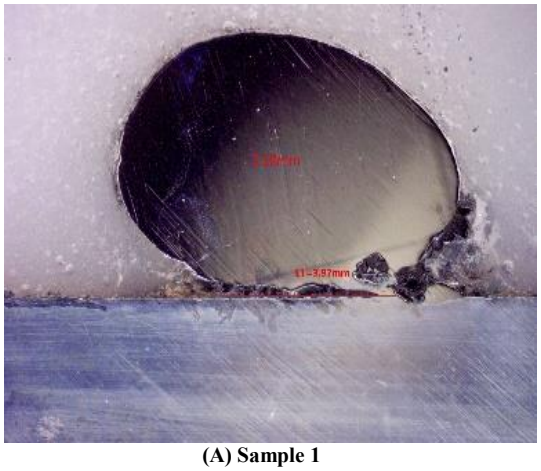

(A) Sample 1

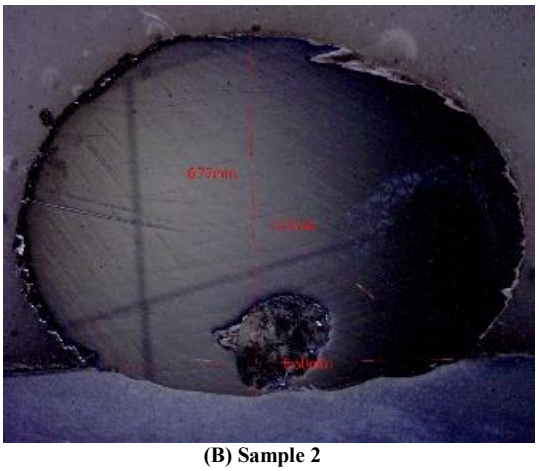

(B) Sample 2

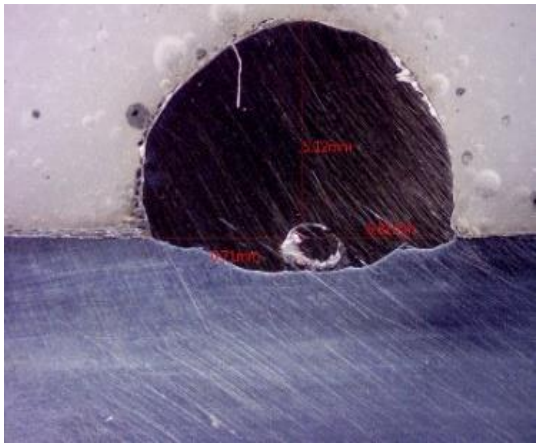

(C) Sample 4

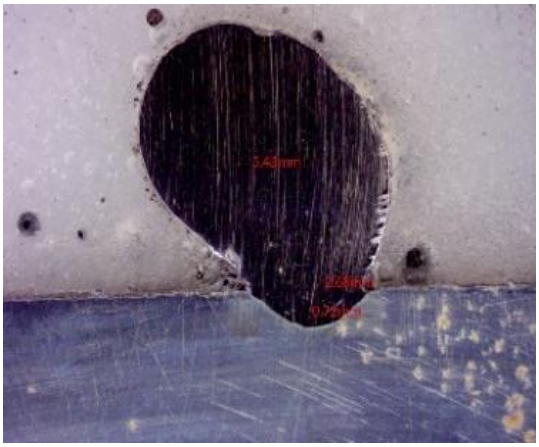

(D) Sample 5

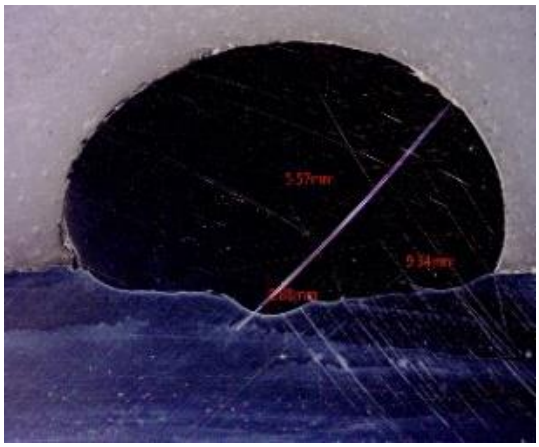

(E) Sample 6

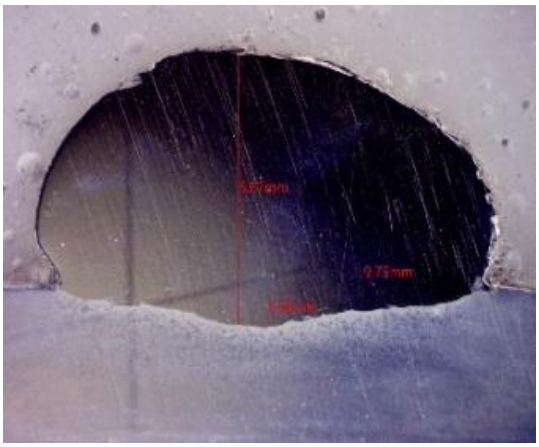

(F) Sample 8

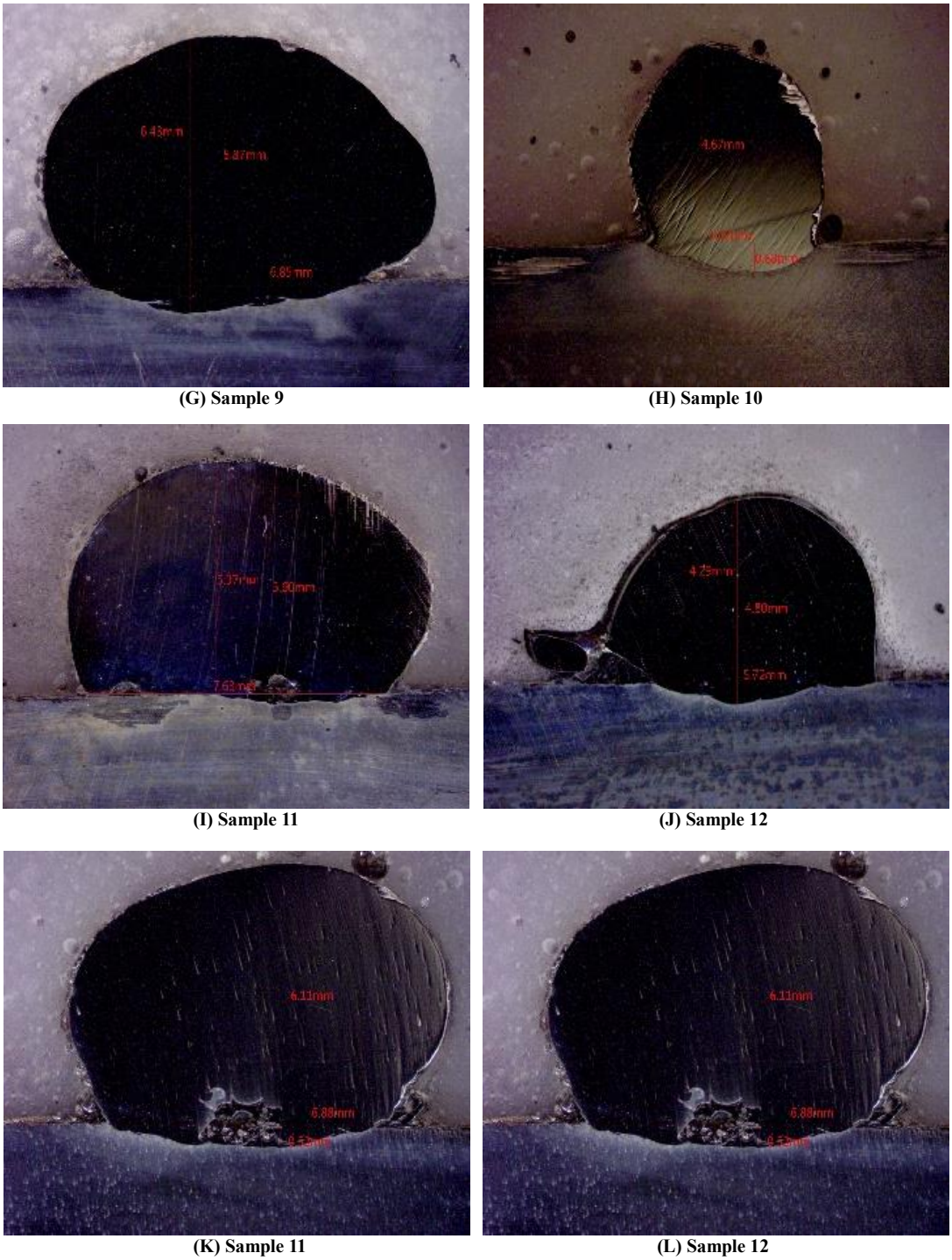

(G) Sample 9 **(H) Sample 10**

(I) Sample 11 **(J) Sample 12**

(K) Sample 11 **(L) Sample 12**

Fig. 11 (A-L) Specimens cross-section of single bead deposition

4. Conclusion

This study intended to evaluate the usefulness of Wire Arc Additive Manufacturing (WAAM) in fabricating 1.14 Cr-1.0 Mo steel adopting flux-cored wires under different conditions. Specifically, the effects of three voltage levels (20, 23, and 26 V), three travel speeds (20, 25, and 30 mm/min), and three gas mixture ratios (1, 5, and 9 L/min) were examined. A total of fifteen experiments were run with the optimization objective of obtaining maximum bead height, minimum bead width, and maximum Depth of Penetration (DOP). The results indicate that the optimal parameters for achieving superior bead width were a voltage of 20 V, a travel speed of 25 m/min, and a gas mixture ratio of 9 L/min. Conversely, the highest bead height and greatest DOP were observed at the highest voltage level (26 V). On the other side, the lowest DOP was observed at 20, 23, and 26 V, and the lowest bead height was observed at these voltage levels.

Further analysis revealed that the combination of a gas mixture ratio of 1 L/min, a speed of travel of 30 mm/min, and a voltage of 26 V or 20 V offers optimal results in terms of the parameters studied. These findings have important implications for the optimization of the WAAM process for

the manufacturing of 1.14 Cr-1.0 Mo low alloy steel components. The optimum parameter obtained through the PVS algorithm is 30m/min travel speed, voltage 23V, and a gas mixture ratio of 3 for manufacturing a multilayer structure.

The optimum parameter obtained through the PVS algorithm is 23V voltage, 30m/min travel speed, and a gas mixture ratio of 3 for manufacturing a multilayer structure. The techniques can be efficient and cost-effective based on the optimization parameters and technique selection.

However, future work can be focused on a composite alloy with optimized parameters to achieve a high-strength-to-weight ratio at a cost-effective price.

Data Availability Statement

All the data is collected from the simulation reports of the software and tools used by the authors. Authors are working on implementing the same using real-world data with appropriate permissions.

Funding

No funds received for this project

Conflicts of Interest

The authors declare that they have no conflict of interest.

Ethical Approval and Human Participation

No ethics approval is required.

References

[1] M. Attaran, "The Rise of 3-D Printing: The Advantages of Additive Manufacturing Over Traditional Manufacturing," *Business Horizons*, vol. 60, no. 5, pp. 677-688, 2017. [CrossRef] [Google Scholar] [Publisher Link]

[2] Barry Berman, "3-D Printing: The New Industrial Revolution," *Business Horizons*, vol. 55, no. 2, pp. 155-162, 2012. [CrossRef] [Google Scholar] [Publisher Link]

[3] Henri Paris et al., "Comparative Environmental Impacts of Additive and Subtractive Manufacturing Technologies," *CIRP Annals*, vol. 65, no. 1, pp. 29-32, 2016. [CrossRef] [Google Scholar] [Publisher Link]

[4] P. Wanjara, M. Brochu, and M. Jahazi, "Electron Beam Freeforming of Stainless Steel using Solid Wire Feed," *Materials & Design*, vol. 28, no. 8, pp. 2278-2286, 2007. [CrossRef] [Google Scholar] [Publisher Link]

[5] Paul A. Colegrove et al., "Microstructure and Residual Stress Improvement in Wire and Arc Additively Manufactured Parts Through High-Pressure Rolling," *Journal of Materials Processing Technology*, vol. 213, no. 10, pp. 1782-1791, 2013. [CrossRef] [Google Scholar] [Publisher Link]

[6] S. Suryakumar et al., "Weld Bead Modeling and Process Optimization in Hybrid Layered Manufacturing," *Computer-Aided Design*, vol. 43, no. 4, pp. 331-344, 2011. [CrossRef] [Google Scholar] [Publisher Link]

[7] Seung Hwan Lee, "Optimization of Cold Metal Transfer-Based Wire Arc Additive Manufacturing Processes Using Gaussian Process Regression," *Metals*, vol. 10, no. 4, pp. 1-13, 2020. [CrossRef] [Google Scholar] [Publisher Link]

[8] Johnnie Liew Zhong Li et al., "Review of Wire Arc Additive Manufacturing for 3D Metal Printing," *International Journal of Automation Technology*, vol. 13, no. 3, pp. 346-353, 2019. [CrossRef] [Google Scholar] [Publisher Link]

[9] Blanka A. Szost et al., "A Comparative Study of Additive Manufacturing Techniques: Residual Stress and Microstructural Analysis of CLAD and WAAM Printed Ti–6Al–4V Components," *Materials & Design*, vol. 89, pp. 559-567, 2016. [CrossRef] [Google Scholar] [Publisher Link]

[10] Ivántabernero et al., "Study on Arc Welding Processes for High Deposition Rate Additive Manufacturing," *Procedia CIRP*, vol. 68, pp. 358-362, 2018. [CrossRef] [Google Scholar] [Publisher Link]

[11] Helen Lockett et al., "Design for Wire + Arc Additive Manufacture: Design Rules and Build Orientation Selection," *Journal of Engineering Design*, vol. 28, no. 7-9, pp. 568-598, 2017. [CrossRef] [Google Scholar] [Publisher Link]

[12] Alessandro Busachi et al., "Designing a WAAM Based Manufacturing System for Defence Applications," *Procedia CIRP*, vol. 37, pp. 48-53, 2015. [CrossRef] [Google Scholar] [Publisher Link]

[13] Lei Yuan et al., "Application of Multidirectional Robotic Wire Arc Additive Manufacturing Process for the Fabrication of Complex Metallic Parts," *IEEE Transactions on Industrial Informatics*, vol. 16, no. 1, pp. 454-464, 2020. [CrossRef] [Google Scholar] [Publisher Link]

[14] Zhuorui Wang et al., "Wire Arc Additive Manufacturing of Network Microstructure (TiB+TiC)/Ti6Al4V Composites using Flux-Cored Wires," *Ceramics International*, vol. 49, no. 3, pp. 4168-4176, 2023. [CrossRef] [Google Scholar] [Publisher Link]

[15] Jay Vora et al., "Optimization of Bead Morphology for GMAW-Based Wire-Arc Additive Manufacturing of 2.25 Cr-1.0 Mo Steel Using Metal-Cored Wires," *Applied Sciences*, vol. 12, no. 10, pp. 1-18, 2022. [CrossRef] [Google Scholar] [Publisher Link]

[16] S.M. Basha et al., "A Review On Severe Plastic Deformation Based Post-Processes for Metal Additive Manufactured Complex Features," *Materials and Manufacturing Processes*, vol. 39, no. 3, pp. 291-309, 2024. [CrossRef] [Google Scholar] [Publisher Link]

[17] Zeqi Hu et al., "Welding Parameters Prediction for Arbitrary Layer Height in Robotic Wire and Arc Additive Manufacturing," *Journal of Mechanical Science and Technology*, vol. 34, pp. 1683-1695, 2020. [CrossRef] [Google Scholar] [Publisher Link]

[18] Leilei Wang, Jiaxiang Xue, and Qiang Wang, "Correlation between Arc Mode, Microstructure, and Mechanical Properties During Wire Arc Additive Manufacturing of 316L Stainless Steel," *Materials Science and Engineering: A*, vol. 751, pp. 183-190, 2019. [CrossRef] [Google Scholar] [Publisher Link]

[19] L.M. Wahsh et al., "Parameter Selection for Wire Arc Additive Manufacturing (WAAM) Process," *Materials Science and Technology*, pp. 78-85, 2019. [CrossRef] [Google Scholar] [Publisher Link]

[20] Subhash Das et al., "Elucidating the Effect of Step Cooling Heat Treatment on the Properties of 2.25 Cr–1.0 Mo Steel Welded with a Combination of GMAW Techniques Incorporating Metal-Cored Wires," *Materials*, vol. 14, no. 20, pp. 1-14, 2021. [CrossRef] [Google Scholar] [Publisher Link]

[21] Muhammad Safwan Mohd Mansor, "Integrated Approach to Wire Arc Additive Manufacturing (WAAM) Optimization: Harnessing the Synergy of Process Parameters and Deposition Strategies," *Journal of Materials Research and Technology*, vol. 30, pp. 2478-2499, 2024. [CrossRef] [Google Scholar] [Publisher Link]

[22] Santosh Kumar Mishra et al., "Wire Arc Additive Manufacturing: Materials, Processes and its Constraints," *Materials and Manufacturing Processes*, vol. 40, no. 69, pp. 723-740, 2025. [CrossRef] [Google Scholar] [Publisher Link]

[23] Harshita Pant et al., "Applications of Wire Arc Additive Manufacturing (WAAM) for Aerospace Component Manufacturing," *The International Journal of Advanced Manufacturing Technology*, vol. 127, pp. 4995-5011, 2023. [CrossRef] [Google Scholar] [Publisher Link]

[24] S.M. Basha et al., "Post-Processing Techniques for Metal Additive Manufactured Products: Role and Contribution of Abrasive Media Assisted Finishing," *Materials and Manufacturing Processes*, vol. 39, no. 6, pp. 737-760, 2024. [CrossRef] [Google Scholar] [Publisher Link]

[25] Rajendra Prasad Meena, N. Yuvaraj, and Vipin, "A Review on Wire Arc Additive Manufacturing based on Cold Metal Transfer," *Materials and Manufacturing Processes*, vol. 39, no. 10, pp. 1315-1341, 2024. [CrossRef] [Google Scholar] [Publisher Link]

[26] Mehrdad Rostami et al., "Review of Swarm Intelligence-Based Feature Selection Methods," *Engineering Applications of Artificial Intelligence*, vol. 100, 2021. [CrossRef] [Google Scholar] [Publisher Link]

[27] John D. Kechagias et al., "3D Printing Parametric Optimization using the Power of Taguchi Design: An Expository Paradigm," *Materials and Manufacturing Processes*, vol. 39, no. 6, pp. 797-803, 2024. [CrossRef] [Google Scholar] [Publisher Link]

[28] Poonam Savsani, and Vimal Savsani, "Passing Vehicle Search (PVS): A Novel Metaheuristic Algorithm," *Applied Mathematical Modelling*, vol. 40, no. 5-6, pp. 3951-3978, 2016. [CrossRef] [Google Scholar] [Publisher Link]

[29] Kishan Fuse et al., "Multi-Response Optimization of Abrasive Waterjet Machining of Ti6Al4V Using Integrated Approach of Utilized Heat Transfer Search Algorithm and RSM," *Materials*, vol. 14, no. 24, pp. 1-22, 2021. [CrossRef] [Google Scholar] [Publisher Link]

[30] E.M. Kasprzak, and K.E. Lewis, "Pareto Analysis in Multiobjective Optimization using the Collinearity Theorem and Scaling Method," *Structural and Multidisciplinary Optimization*, vol. 22, pp. 208-218, 2001. [CrossRef] [Google Scholar] [Publisher Link]